Title
Ultra-Sensitive Graphene-Plasmonic Hybrid Platform for Label-Free Detection

Journal
Advanced Materials, 25(35)

ISSN
0935-9648

Authors
Wang, Pu
Liang, Owen
Zhang, Wei
et al.

Publication Date
2013-09-20

DOI
10.1002/adma.201300635

Peer reviewed

Ultra-Sensitive Graphene-Plasmonic Hybrid Platform for Label-Free Detection

*Pu Wang, Owen Liang, Wei Zhang, Thomas Schroeder, and Ya-Hong Xie**

Surface-enhanced Raman scattering (SERS), capable of label-free single molecule detection and providing high-resolution vibrational information, is one of the most powerful analytical techniques.[1–3] Various metallic nanostructures with tunable plasmonic properties have been explored as SERS active substrates.[4–6] Enormous electromagnetic enhancement required to reach analytical limits is induced at the space in between nanoparticles (hot spots).[7] An ideal platform for SERS-based single molecule detection (SM-SERS) is expected to be reproducible, chemically stable, biological compatible, and should be easily fabricated at the scale of manufacturing. Though the detailed physical mechanism of SERS is still under debate, it has been widely accepted that SERS enhancement results from a combination of electromagnetic mechanism (EM) and chemical mechanism (CM).[8] EM[9] originates from the orders-of-magnitude increase in the local (non-propagating) electromagnetic field due to plasmonic resonance, while CM[10] is caused by charge transfer between the molecules under study and the substrate. The SERS enhancement of EM can reach up to 10^{14} while that of CM is ~10–100.[10,11]

Graphene, with its unique optical, electronic and mechanical properties,[12–14] holds promises for applications in photonics and optoelectronics. The combination of graphene with plasmonic nanostructures (ranging from nanoparticles, nano-antennas to quantum dots) has been shown to largely expand and complement graphene's applications in photodetector,[15–17] optical modulator,[18] polarizer,[19] phototransistor[20] and plasmon resonance sensor.[21] However, SM-SERS employing graphene has not been fully explored. A number of reports have appeared in the literature on the potential in sensitive and selective detection of protein and DNA using various graphene platforms.[22–26] Graphene has also been shown to be superior to metallic surfaces in terms of bio-compatibility and chemical-stability.[27,28] Molecular charge transfer between molecules and graphene has been shown to be significant for selected families of molecules.[29–31] These properties make it possible to study and modulate SERS effects using graphene superimposed over nano-structured metallic surfaces. Graphene has indeed the promise as a very important building block in SERS active structures especially for biosensing applications.

Here, we present a graphene-Au nano-pyramids hybrid system with demonstrated single molecule sensitivity. The graphene hybrid system boosts a high density of hot spots with local SERS enhancement factor of over 10^{10} for rhodamine 6G (R6G) as well as lysozyme, and enables label-free sensing. The specific fabrication approach of the Au nano-pyramids is amenable to engineering the SERS hotspots in terms of their density and location *via* lithography. The coincidence of molecular precipitation region with SERS hot spots makes detection of a few or a single molecule possible.[32–34] Single molecule SERS detection is demonstrated experimentally using a bi-analyte approach.[35–37] Furthermore, the high resolution vibrational information provided by SERS enables us to better understand the chemical mechanism, and explore the interaction between molecules and graphene.

In our approach we used a hybrid SERS-active platform consisting of a single layer graphene (SLG) covering a quasi-periodic Au nano-pyramid (also referred to as Au tips) arrays,[38] as illustrated in **Figure 1**a. The hexagonally arranged sharp Au tips, almost identical in size and topology, support markedly enhanced local fields and play a key role in the ultrahigh sensitive system. The tipped substrate can be fabricated in large scale with superior reproducibility (Figure 1b). Figure 1c shows the scanning electron microscopy (SEM) image of the hybrid structure. The CVD SLG sheet was transferred to tipped surface using PMMA.[39] Graphene deforms itself to conform to the substrate geometry *via* van der Waals force.

We demonstrated SERS using two types of molecules with the graphene based hybrid platform (**Figure 2**). Lysozyme, a type of simple protein commonly used as the standard in the study of bio-molecules, is used. The active fluorescent molecule R6G is also used as a reference. Figure 2a-b show the average Raman intensities of R6G and lysozyme deposited on the graphene-based hybrid platform at various molecular concentrations. We achieved R6G SERS with concentration down to 10^{-14} M (equivalent to ~0.0015 molecules per μm^2 on average of the surface area) as well as lysozyme with concentration as low as 10^{-12} M (~0.15 molecules per μm^2 of the surface area). The detection efficiency can be markedly increased with the help of graphene over Au pyramids. The local variation of the intensity of graphene characteristic Raman peaks can be used as markers for locating hot spots where the Raman signal of the molecules is also the strongest (see Supporting Information). At low concentration limits such as 10^{-14} M, the knowledge of the location of the hot spots greatly shortens the time it takes to locate the sparse molecular Raman signal. The presence of SLG is evidenced by the characteristic D, G, and 2D bands.[40] The prominent D-band has been shown to result from the 1D graphene folds as opposed

P. Wang, O. Liang, W. Zhang, Prof. Dr. Y. -H. Xie
Department of Materials Science and Engineering
and California Nano Systems Institute (CNSI)
University of California
Los Angeles, Los Angeles, CA 90095-1595, USA
E-mail: yhx@ucla.edu
Prof. Dr. T. Schroeder
Department Materials Research
IHP, Im Technologiepark 25, Frankfurt (Oder), D-15236, Germany

DOI: 10.1002/adma.201300635

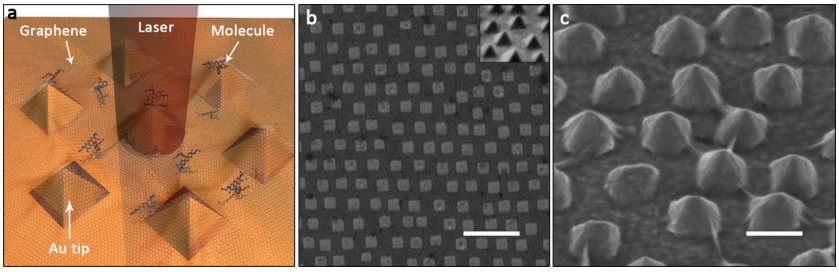

Figure 1. a) Schematic illustration of Raman experiments of molecules on the graphene-Au nano-pyramid (tip) hybrid structure; b) SEM image of the semi-periodic array of Au tips. Scale bar, 1 μm; c) SEM image of hexagonally arranged arrays of Au tips with sharply folded graphene; scale bar, 200 nm.

to broken carbon bonds.[41] The same experiments performed with Au tip surfaces free of graphene also resulted in substantial enhancement (Figure 2c-d), indicating the crucial role of the periodic Au tip surface for the high sensitivity. The average Raman intensities of both R6G and lysozyme are further enhanced (by approximately a factor of 10) by covering the Au tipped surfaces with graphene, and the enhancement factors vary with different Raman vibrational modes. It has been reported that monolayer graphene facilitates charge transfer between graphene and probe molecules, resulting in a vibration-mode dependent enhancement of 2–17 times.[42] As will be shown, such variation in CM enhancement factor allows us to probe in further details of the different vibration modes of individual molecules.

We analyzed different vibrational modes of R6G and lysozyme deposited on Au tip substrate with and without graphene (**Figure 3**a). Figure 3b shows a comparison of the R6G peaks at 613 cm^{-1} and 1187 cm^{-1}. The peak at 613 cm^{-1} is assigned to the C-C-C deformation in-plane vibration and the peak at 1187cm^{-1} is assigned to the in-plane vibration of deformed C-H bonds.[43,44] They are slightly shifted from the typical 612 cm^{-1} and 1185 cm^{-1} position due presumably to the extremely high local electric field associated with the plasmonic resonance.[45] The 613 cm^{-1} peak intensity is enhanced by a factor of 10 with the presence of graphene, while the 1187 cm^{-1} peak intensity is only enhanced by a factor of 5 for a R6G concentration of 10^{-12} M. Similar behavior is also observed for lysozyme.[46] As shown in Figure 3c, the band at 1060 cm^{-1} exhibits a larger enhancement than the peak at 1466 cm^{-1}.

The dependence of the graphene-derived CM enhancement factor for various vibrational modes is shown quantitatively in Supporting Information. The peak at 613 cm^{-1} and the 1577 cm^{-1} peak assigned separately to C-C-C and C-O-C bond stretching vibrations show the highest enhancement ($I_{G/Tip}/I_{Tip}$ ~9). The peaks at 1311, 1360, 1506, and 1645 cm^{-1} assigned to C-C stretching modes show 4-6 folds enhancement. The peak at 775 cm^{-1} assigned to the out-of-plane vibration of deformed C-H bonds shows an average enhancement of 5 times. Among all peaks, the peak at 1187 cm^{-1} assigned to in-plane C-H stretching modes exhibits the lowest enhancement (~2 times). For lysozyme, the band at 1060 cm^{-1} assigned to the vibrations of ν(C-N) is about 3-fold more enhanced than the $\delta(CH_2)$ vibration mode[48] observed at 1466 cm^{-1}.

These observations allow us to propose the following mechanisms for the SERS chemical enhancement attributed to graphene-molecule interaction. Firstly, the 2–10 times enhancement for all vibration modes partly result from charge transfer between molecules and graphene.[42,47] Charge transfer occurs when the graphene Fermi level is located in between the HOMO and LUMO of molecules including R6G[47] (Figure 3d). Secondly, aromatic molecules prefer to stack in parallel to the π-bonds of graphene through π–π stacking and lead to enhanced resonant energy transfer.[49,50] In our experiments of lysozyme, the absence of peaks assigned to the symmetric ring-breathing vibration mode (exist only when benzene rings stand up or at least be tilted with respect to the surface)[46] reflects the flat orientation of the aromatic amino acid residues in lysozyme. Both charge transfer and resonant energy transfer effects are expected to be stronger when molecules are closer to the surface. In the case of charge transfer, the increased separation between negative and positive charges leads to an increase in molecular polarizability

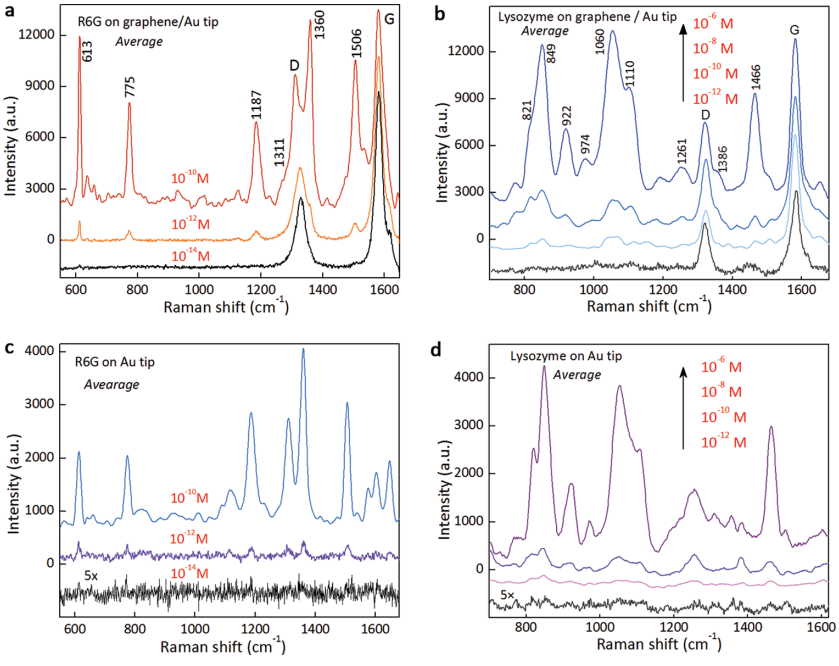

Figure 2. a) Raman spectra of R6G on graphene hybrid structure with 3 different concentrations (10^{-10} M, ~15 molecules/μm^2 10^{-12} M, ~0.15 molecules/μm^2, 10^{-14} M, ~0.0015 molecules/μm^2) b) Raman spectra of lysozyme on graphene hybrid structure with 4 different concentrations (10^{-6} M, 10^{-8} M, 10^{-10} M, 10^{-12} M). c) Raman spectra of R6G on Au tips with 3 different concentrations. d) Raman spectra of lysozyme on Au tips with 4 different concentrations. The laser excitation wavelength is 633 nm.

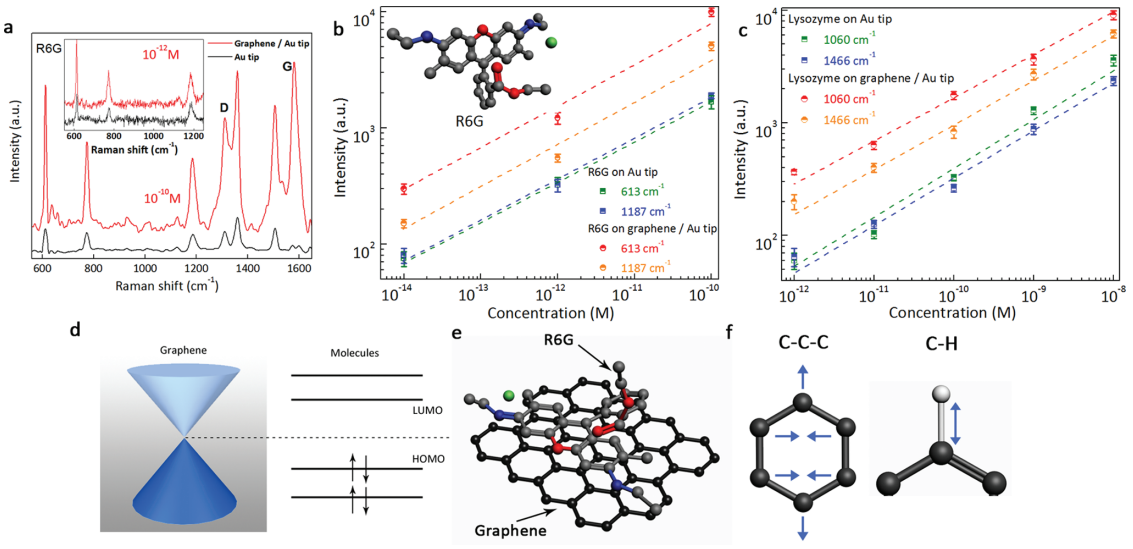

Figure 3. a) Raman spectra of R6G on graphene hybrid structure and Au tips at molecular concentrations 10^{-10} M and 10^{-12} M. b) The Raman intensity of R6G peaks at 613 $cm^{-1}$and 1087 cm^{-1} on graphene hybrid structure and Au tips separately, as a function of the molecular concentration, in log scale. c) Raman intensity of lysozyme peaks at 1060 cm^{-1} and 1466 cm^{-1} on graphene hybrid structure and Au tips separately, as a function of the molecular concentration, in log scale. d) Energy level diagram of graphene–molecule interface: charge transfer occurs when graphene Fermi level locates in between the HOMO and LUMO of molecules. e) Schematic of a R6G molecule lying parallel to graphene surface. f) Schematic of in-plane deformation C-C-C vibration mode and in-plane deformation C-H vibration mode of R6G molecules.

that has been associated with larger Raman scattering cross-sections.[10] Furthermore, the basic chemical structures of R6G are similar to that of graphene, thus the in-plane deformation C-C-C vibrational mode will be further enhanced due to the vibrational coupling between the molecules and graphene. In contrast, such effects are absent for the deformed C-H in-plane vibrational mode. This explains the more pronounced enhancement of the 613 cm^{-1} peak assigned to the in-plane deformation C-C-C vibration. The behavior of the enhancement factors being dependent on the geometry of the molecules is a distinct characteristic of SERS chemical mechanisms. A more in-depth study of graphene-based surface enhancement scattering (GERS) has been given in ref. 47.

Single molecule detection was demonstrated with bi-analyte SERS (BiASERS) method. The BiASERS method is a contrast based spectroscopy technique using two different molecules at the same time. This approach facilitates reliable statistics based on a large spectral sample size for single molecule SERS detection. In our case, an aqueous solution of rhodamine 6G (R6G) and lysozyme of the same concentration was dispensed on the hybrid platform for SM-SERS under 633 nm excitation. The significant difference between R6G and lysozyme's Raman fingerprints makes them highly distinguishable. Spatially resolved Raman mappings of R6G and lysozyme were measured for three progressively diluted analyte solutions (10^{-8} M, 10^{-10} M, 10^{-12} M). (see Supporting Information). Raman intensity mappings of selected molecular vibration modes (R6G band at 613 cm^{-1} and lysozyme band at 821 cm^{-1}) at 10^{-10} M and 10^{-12} M concentrations are shown in **Figure 4**a-d. When solution concentration is further reduced, percentage of overlapping R6G-lysozyme signal significantly decreases, and breakdown of ensemble averaging spectra occurs when single molecule regime has been reached (Figure 4e). We observed signal purely composed of SERS spectrum of one type of molecule, shown as a rather isolated pixel in the mapping. At extreme dilution, the spatial coincidence of an analyte molecule with the hot spots of the hybrid platform will be the key to detect molecular signal. Following the argument of Le Ru and Etchegoin,[35–37] the bi-analyte nature of target molecules serves as strong evidence that the spectrum of one certain analyte from an individual pixel is attributed to single molecule.

Next, we present spatially resolved Raman data to assess the relative importance of EM and CM to the overall SERS enhancement (**Figure 5**). Comparing the Raman intensity mapping of R6G 613cm^{-1} peak with that of the graphene G peak (Figure 5a inset), we find that the hotspots coincide. Figure 4a shows the Raman spectra of R6G at three spots on the graphene hybrid platform, two of them are from the hotspots in the mapping. Figure 5b shows the Raman intensities of R6G 613 cm^{-1} peak and 1187cm^{-1} peak as a function of graphene G peak intensity. The intensities of the R6G characteristic peaks correspond linearly to the graphene G band intensity. The lysozyme–graphene peak intensities from a series of spectra of a line scan over one of the hotspots are shown in Figure 5c, which also shows the same linear dependence. The linear dependence spans significantly over 3 orders of magnitude. The observations of synchronized enhancement of the molecular and the graphene Raman peaks serve as strong evidence that the significant local EM field enhancement from the Au nanostructures is the major contribution to the dramatically enhanced Raman signals, in agreement with other SERS studies.[51,52]

The precise location of the SERS hot spots relative to the location and the orientation of the nano-pyramids are studied both experimentally and theoretically. **Figure 6**a shows the spatially resolved Raman spectra of graphene 2D band intensity. Within the diffraction limited spatial resolution of the 633 nm

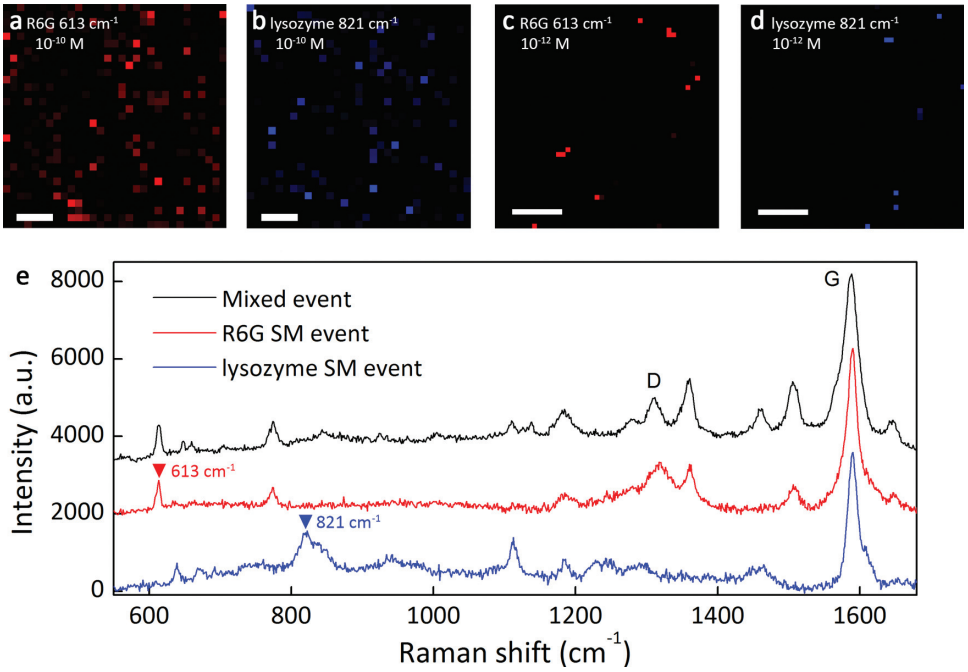

Figure 4. Spatial resolved Raman intensity mapping and selected spectra of R6G and lysozyme bianalyte mixture on hybrid platform at different concentrations. (a), R6G peak at 613 cm^{-1}(red) and (b), Lysozyme peak at 821 cm^{-1}(blue) intensity mappings of the same area at 10^{-10} M. Scale bar: 10 µm. (c), R6G peak at 613 cm^{-1}(red) and (d), Lysozyme peak at 821 cm^{-1}(blue) intensity mappings of the same area at 10^{-12} M. Scale bar: 10 µm. (e), Selected spectra from the mapping area. Bi-analyte mixed event: black. R6G single molecule event: red. Lysozyme single molecule event: blue.

excitation laser, the hotspots appear to be located in between Au tips. We modeled the enhancement of the electric field of Au nano-pyramids using Finite-difference time-domain (FDTD) analysis (see Methods). The hexagonally arranged 200 nm Au nano-pyramids geometry representative of the actual sample structure was used. Figure 6b-c shows the x-z and x-y views of the electric field amplitude distribution for incident light wavelength 633 nm. Strong field enhancement appears in between two individual tips as well as at the apex. However, the volume of the high field region in between the tips is approximately one order of magnitude larger compared to that at the apex and is expected to be the dominant contributor to the detected Raman signal. The hot spots distribution in the Raman map (Figure 6a) provides strong support to the above

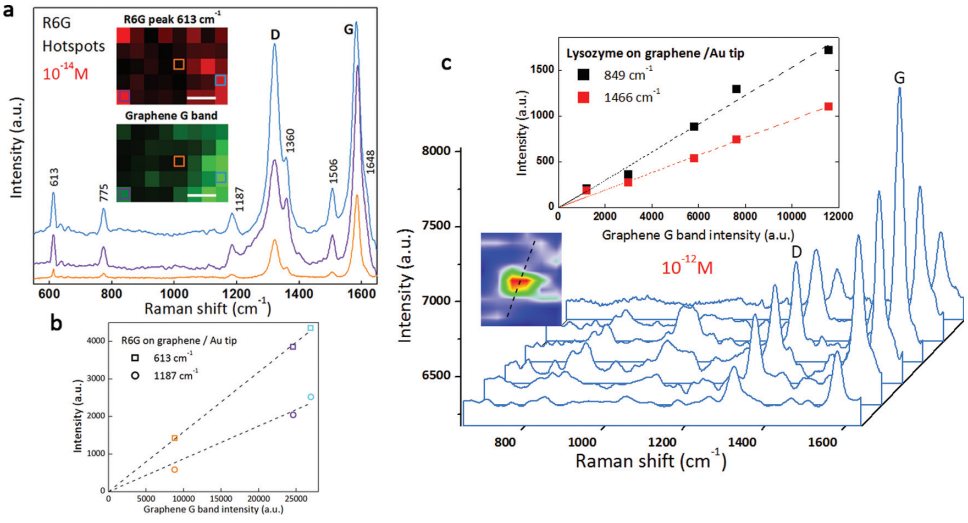

Figure 5. a) SERS spectra for 10^{-14} M R6G on graphene hybrid system taken from three spots from the inset Raman mappings in the same color squares. The inset of panel (a) is composed of Raman intensity mapping of R6G peak at 613 cm^{-1} (red) and Raman intensity mapping of graphene G band (green), scale bar, 2 µm. b) Raman intensities of R6G peaks at 613 cm^{-1} and 1187 cm^{-1} separately as a function of graphene G band from the three spectra shown in panel (a). c) A series of Raman spectra from a line scan across a lysozyme SERS hotspot. The spectral interval is 500 nm. Inset: Raman intensities of lysozyme peaks at 849 cm^{-1} and 1466 cm^{-1} separately as a function of graphene G band from the spectra shown in panel (c).

ADVANCED MATERIALS
www.advmat.de

www.MaterialsViews.com

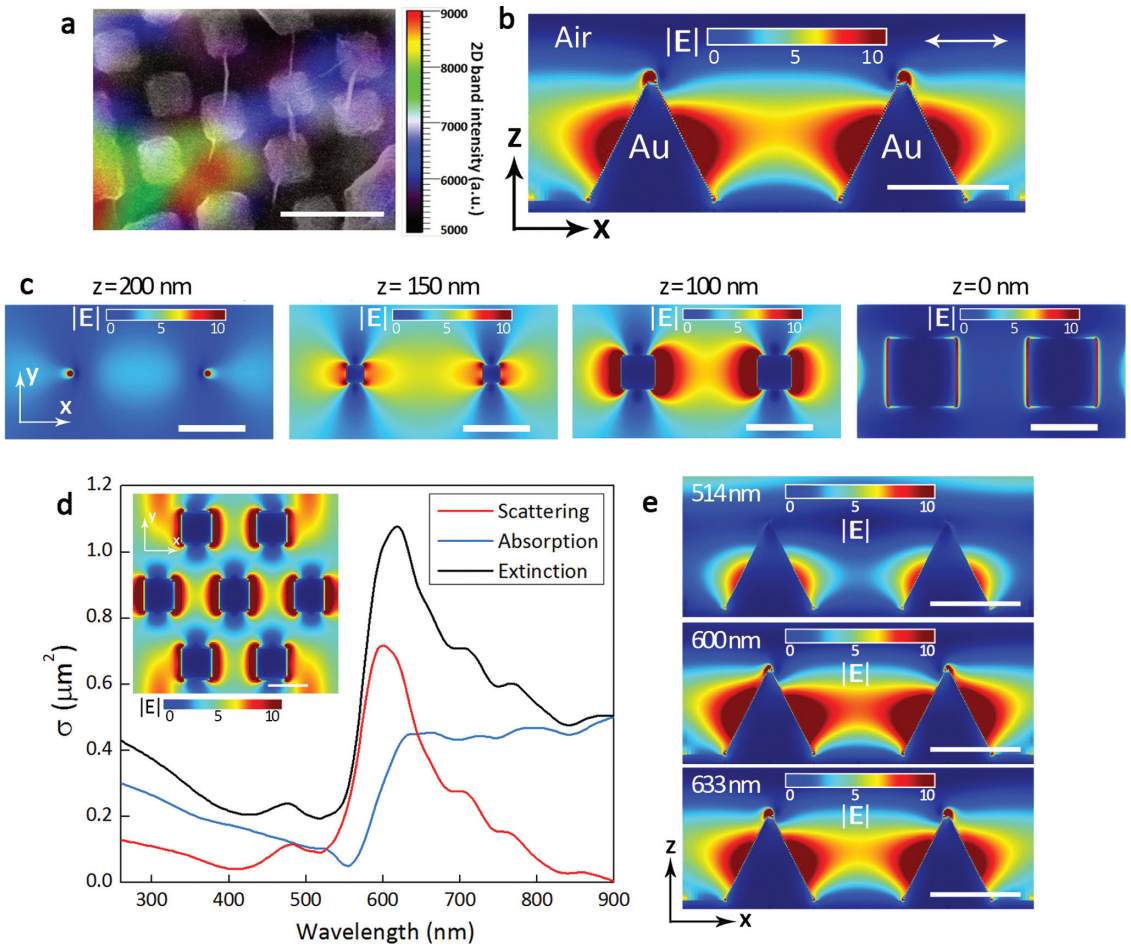

Figure 6. a) Raman mapping of graphene 2D band intensity for the hybrid structure. Scale bar, 500 nm. FDTD simulated b) x-z view of electric field distribution between two Au tips in the periodic structure. The incident light wavelength is 633 nm. The white arrow indicates the polarization direction of the incident light. Scale bar, 200 nm. c) x-y view of electric field distribution between two Au tips when z = 200, 150, 100, 0 nm separately. Scale bar, 200 nm. d) FDTD-simulated extinction (black line), absorption (blue line) and scattering (red line) cross-sections and electric field distribution of periodic hexagonally arranged Au tips. Scale bar, 200 nm. e) x-z view of electric field distribution between two Au tips with incident light λ = 514 nm, 600 nm, 633 nm. Scale bar, 200 nm.

expectation and is in excellent agreement with the modeling results. The regions of strong fields represent evanescent (non-propagating) modes of the plasmonic structure with only near-field coupling capability.[53]

To obtain a consistent picture of plasmonic resonance, both near field as well as far field optical responses are needed. Figure 6d shows the simulated far field extinction spectra as well as near field electric field distribution of the tip substrate. The extinction peak can be decomposed into absorption and scattering contributions. The hexagonally arranged Au tip substrate exhibits an extinction peak at ≈600 nm, with FWHM ≈100 nm. The simulated field intensity maps in Figure 6e also show the wavelength dependence with a clear peak characteristic of resonant behavior.

In summary, we have developed a bio-compatible graphene based SERS active platform that enables single molecule detection and provides a reproducible and uniform response. The hybrid substrate generates a high density of "hot spots" with SERS enhancement factors over 10^{10}. The addition of graphene allows us to determine separately chemical enhancement (CM) and electromagnetic enhancement (EM) in a semi-quantitative fashion. In practical applications, the option of adding graphene to SERS active metallic surfaces will broaden the utility of such platforms by offering chemically inert surface that is easily refreshed after each test and also being resistant to the degradation of the metallic nano-structures.[54] The result indicates that EM is the dominant contributor with CM adding another order of magnitude to the large SERS enhancement factor. Our approach and the results will go beyond simple single molecule detection to facilitate understanding of the basic mechanisms of SERS, and open up new opportunities in developing and revolutionizing the applications of graphene in biomedical diagnostics, analytical chemistry, as well as biological sensing and imaging.

Experimental Section

Sample fabrication: The periodic Au nano-pyramid structure with tunable size and sharpness can be fabricated by a wafer-scale

templating technology.[55,56] Spin-coated on (001) silicon wafers, close-packed monolayer polystyrene balls of ~200 nm diameter serve as templates. The templated chromium nano-hole arrays can be used as etching masks. Then periodic inverted silicon pyramidal pits are created by anisotropic etching in KOH solutions since KOH preferentially etches silicon in the (001) plane. Wafer-scale gold nano-pyramid arrays can be fabricated by the silicon templates with inverted pyramidal pits through an adhesion and peeling process. The silicon templates with inverted pyramidal pits are employed as reusable structural templates to replicate arrays of metallic nano-pyramids with sharp tips.

Micro-Raman spectroscopy: Micro-Raman spectra and mapping of molecules and graphene were carried out using a Renishaw inVia Raman Spectroscope under ambient conditions. The laser excitation wavelength is 633 nm from a He-Ne laser. The power of the laser was kept around 1.5 mW for single spectrum and 0.5 mW for mapping to avoid sample heating. The laser spot size was ~0.5 μm. We used a ×100 objective (numerical aperture 0.90) and spectral analysis was accomplished with a 1800 lines per mm grating. The spectroscope is equipped with a High Speed Encoded Stage that enables shift of samples in XYZ directions with nominal spatial resolution of ~100 nm. The spatially-resolved Raman mapping data is achieved by Raman imaging with step down to 0.2 μm in X and Y direction with the actual spatial resolution being limited by diffraction. The Raman imaging data is processed by WiRE 3.2 Raman software.

FDTD: simulations Three-dimensional FDTD simulations were performed using a commercial software (FDTD Solutions, Lumerical Inc.). A conformal mesh with size down to 0.5 nm (x, y and z directions) was used. The optical constants of Au were taken from E. Palik[57] in the spectrum range of 200 nm to 1000 nm. Perfectly matched layer (PML) boundary condition was applied for z-direction, while periodic boundary condition was set for x and y directions of the FDTD simulation region. The amplitude $|E_0|$ of incident light is 1.

Supporting Information

Supporting Information is available from the Wiley Online Library or from the author.

Acknowledgements

The authors acknowledge the support from Function Accelerated nanoMaterial Engineering (FAME) and California NanoSystems Institute (CNSI). P.W. and Y.H.X. would like to thank Dr. Wolfgang Mehr of IHP for his encouragement and facilitating the experiments, and Grzegorz Kozlowski of IHP for his help related to the use of the Raman spectroscopy. Y.H.X. acknowledges the support from Alexander von Humboldt Foundation Research Award that made this research possible.

Received: February 6, 2013
Revised: April 6, 2013
Published online: August 6, 2013

[1] K. Kneipp, Y. Wang, H. Kneipp, L. T. Perelman, I. Itzkan, R. R. Dasari, M. S. Feld, *Phys. Rev. Lett.* **1997**, *78*, 1667–1670.
[2] S. Nie, S. R. Emory, *Science* **1997**, *275*, 1102–1106.
[3] N. P. W. Pieczonka, R. F. Aroca, *Chem. Soc. Rev.* **2008**, *37*, 946–954.
[4] H. W. Liu, L. Zhang, X. Y. Lang, Y. Yamaguchi, H. Iwasaki, Y. Inouye, Q. K. Xue, M. W. Chen, *Sci. Rep.* **2011**, *1*, 112.
[5] D. K. Lim, K. S. Jeon, J. H. Hwang, H. Kim, S. Kwon, Y. D. Suh, J. M. Nam, *Nat. Nanotechnol.* **2011**, *6*, 452–460.
[6] J. F. Li, Y. F. Huang, Y. Ding, Z. L. Yang, S. B. Li, X. S. Zhou, F. R. Fan, W. Zhang, Z. Y. Zhou, D. Y. Wu, B. Ren, Z. L. Wang, Z. Q. Tian, *Nature* **2010**, *464*, 392–395.
[7] S. Lal, N. K. Grady, J. Kundu, C. S. Levin, J. B. Lassiter, N. J. Halas, *Chem. Soc. Rev.* **2008**, *37*, 898–911.
[8] A. Campion, P. Kambhampati, *Chem. Soc. Rev.* **1998**, *27*, 241–250.
[9] H. Xu, J. Aizpurua, M. Kall, P. Apell, *Phys. Rev. E* **2000**, *62*, 4318.
[10] B. N. J. Persson, K. Zhao, Z. Zhang, *Phys. Rev. Lett.* **2006**, *96*, 207401.
[11] A. Otto, I. Mrozek, H. Grabhorn, W. J. Akemann, *Phys: Condens. Matter* **1992**, *4*, 1143.
[12] F. Bonaccorso, Z. Sun, T. Hasan, A. C. Ferrari, *Nat. Photon.* **2010**, *4*, 611–622.
[13] A. H. C. Neto, F. Guinea, N. M. R. Peres, K. S. Novoselov, A. K. Geim, *Rev. Mod. Phys.* **2009**, *81*, 109–162.
[14] C. G. Lee, X. D. Wei, J. W. Kysar, J. Hone, *Science* **2008**, *321*, 385–388.
[15] F. N. Xia, T. Mueller, Y. M. Lin, A. Valdes-Garcia, P. Avouris, *Nat. Nanotechnol.* **2009**, *4*, 839–843.
[16] T. Mueller, F. N.Xia, P. Avouris, *Nat. Photon.* **2010**, *4*, 297–301.
[17] Z. Y. Fang, Z. Liu, Y. M. Wang, P. M. Ajayan, P. Nordlander, N. J. Halas, *Nano Lett.* **2012**, *12*, 3808–3813.
[18] M. Liu, X. B. Yin, X. Zhang, *Nano Lett.* **2012**, *12*, 1482–1485.
[19] Q. L. Bao, H. Zhang, B. Wang, Z. H. Ni, C. H. Lim, Y. Wang, D. Y. Tang, K. P. Loh, *Nat. Photon.* **2011**, *5*, 411–415.
[20] G. Konstantatos, M. Badioli, L. Gaudreau, J. Osmond, M. Bernechea, F. P. Garcia de Arquer, F. Gatti, F. H. L. Koppens, *Nat. Nanotechnol.* **2012**, *7*, 363–368.
[21] O. Salihoglu, S. Balci, C. Kocabas, *Appl. Phys. Lett.* **2012**, *100*, 213110.
[22] V. C. Sanchez, A. Jachak, R. H. Hurt, A. B. Kane, *Chem. Res. Toxicol.* **2012**, *25*, 15–34.
[23] Y. Wang, Z. H. Li, J. Wang, J. H. Li, Y. H. Lin, *Trends Biotechnol.* **2011**, *29*, 205–212.
[24] E. Dubuisson, Z. Y. Yang, K. P. Loh, *Anal. Chem.* **2011**, *83*, 2452–2460.
[25] M. Bonanni, M. Pumera, *ACS Nano.* **2011**, *5*, 2356–2361.
[26] O. Akhavan, E. Ghaderi, R. Rahighi, *ACS Nano* **2012**, *6*, 2904–2916.
[27] S. S. Chen, L. Brown, M. Levendorf, W. W. Cai, S. Y. Ju, J. Edgeworth, X. S. Li, C. W. Magnuson, A. Velamakanni, R. D. Piner, J. Y. Kang, J. W. Park, R. S. Ruoff, *ACS Nano* **2011**, *5*, 1321–1327.
[28] D. W. Kang, J. Y. Kwon, H. Cho, J. H. Sim, H. S. Hwang, C. S. Kim, Y. J. Kim, R. S. Ruoff, H. S. Shin, *ACS Nano* **2012**, *6*, 7763–7769.
[29] R. S. Swathi, K. L. Sebastian, *J. Chem. Phys.* **2008**, *129*, 054703.
[30] J. T. Sun, Y. H. Lu, W. Chen, Y. P. Feng, A. T. S. Wee, *Phys. Rev. B.* **2010**, *81*, 155403.
[31] M. Lopes, A. Candini, M. Urdampilleta, A. Reserbat-Plantey, V. Bellini, S. Klyatskaya, L. Marty, M. Ruben, M. Affronte, W. Wernsdorfer, N. Bendiab, *ACS Nano* **2010**, *4*, 7531–7537.
[32] A. M. Michaels, M. Nirmal, L. E. Brus, *J. Am. Chem. Soc.* **1999**, *121*, 9932–9939.
[33] N. P. W. Pieczonka, Ricardo F. Aroca, *Chem. Soc. Rev.* **2008**, *37*, 946–954.
[34] F. De Angelis, F. Gentile, F. Mecarini, G. Das, M. Moretti, P. Candeloro, M. L. Coluccio, G. Cojoc, A. Accardo, C. Liberale, R. P. Zaccaria, G. Perozziello, L. Tirinato, A. Toma, G. Cuda, R. Cingolani, E. Di Fabrizio, *Nat. Photonics* **2011**, *5*, 682–687.
[35] E. C. Le Ru, M. Meyer, P. G. Etchegoin, *J. Phy. Chem. B* **2006**, *110*, 1944–1948.
[36] P. G. Etchegoin, M. Meyer, E. Blackie, E. C. Le Ru, *Anal. Chem.* **2007**, *79*, 8411.
[37] P. G. Etchegoin, E. C. Le Ru, A. Fainstein, *Phys. Chem. Chem. Phys.* **2011**, *13*, 4500–4506.
[38] J. Y. Lee, K. Sun, B. Y. Li, X. Y. Wei, T. P. Russel, Y. H. Xie, *IEEE Trans. Nanotechnol.* **2011**, *10*, 256.
[39] X. S. Li, W. W. Cai, J. H. An, S. Y. Kim, J. H. Nah, D. X. Yang, R. Piner, A. Velamakanni, I. Jung, E. Tutuc, S. K. Banerjee, L. Colombo, R. S. Ruoff, *Science.* **2009**, *324*, 1312–1314.

[40] A. C. Ferrari, J. C. Meyer, V. Scardaci, C. Casiraghi, M. Lazzeri, F. Mauri, S. Piscanec, D. Jiang, K. S. Novoselov, S. Roth, A. K. Geim, *Phys. Rev. Lett.* **2006**, *97*, 187401.
[41] P. Wang, W. Zhang, O. Liang, M. Pantoja, J. Katzer, T. Schroeder, Y. H. Xie, *ACS Nano.* **2012**, *6*, 6244.
[42] X. Ling, L. M. Xie, Y. Fang, H. Xu, H. L. Zhang, J. Kong, M. S. Dresselhaus, J. Zhang, Z. F. Liu, *Nano Lett.* **2010**, *10*, 553–561.
[43] J. Zhao, O.Chen, D. B. Strasfeld, M. G. Bawendi, *J. Am. Chem. Soc.* **2007**, *129*, 7647–7656.
[44] A. M. Michaels, J. Jiang, L. J. Brus, *J. Phys. Chem. B.* **2000**, *104*, 11965–11971.
[45] T. R. Jensen, M. D. Malinsky, C. L. Haynes, R. P. Van Duyne, *J. Phys. Chem. B.* **2000**, *104*, 10549.
[46] J. Hu, R. S. Sheng, Z. S. Xu, Y. E. Zeng, *Spectrochim. Acta* **1995**, *51*, 1087–1096.
[47] X. Ling, L. G. Moura, M. A. Pimenta, J. Zhang, *J. Phys. Chem. C* **2012**, *116*, 25112.
[48] S. K. Kim, M. S. Kim, S. W. Suh, *J. Raman Spectrosc.* **1987**, *18*, 171–175.
[49] A. Rochefort, J. D. Wuest, *Langmuir.* **2009**, *25*, 210–215.
[50] Y. Uehara, S. Ushioda, *Appl. Phys. Lett.* **2005**, *86*, 181905.
[51] T. J. Echtermeyer, L. Britnell, P. K. Jasnos, A. Lombardo, R. V. Gorbachev, A. N. Grigorenko, A. K. Geim, A. C. Ferrari, K. S. Novoselov, *Nat. Commun.* **2011**, *2*, 458.
[52] F. Schedin, E. Lidorikis, A. Lombardo, V. G. Kravets, A. K. Geim, A. N. Grigorenko, K. S. Novoselov, A. C. Ferrari, *ACS Nano* **2010**, *4*, 5617–5626.
[53] W. Zhou, T. W. Odom, *Nat. Nanotechnol.* **2011**, *6*, 423–427.
[54] J. S. Bunch, S. S. Verbridge, J. S. Alden, A. M. van der Zande, J. M. Parpia, H. G. Craighead, P. L. McEuen, *Nano Lett.* **2008**, *8*, 2458–2462.
[55] C. H. Sun, N. C. Linn, P. Jiang, *Chem. Mater.* **2007**, *19*, 4551–4556.
[56] K. Sun, J. Y. Lee, B. Y. Li, W. Liu, C. Q. Miao, Y. H. Xie, X. Y. Wei, T. P. Russell, *J. Appl. Phys.* **2010**, *108*, 036102–036104.
[57] E. D. Palik, *Handbook of Optical Constants of Solids*, Elsevier Inc. **1997**.